



HAL
open science

Short term reliability and robustness of ultra-thin barrier, 110 nm-gate AlN/GaN HEMTs

Zhan Gao, Matteo Meneghini, Kathia Harrouche, Riad Kabouche, Francesca Chiocchetta, Etienne Okada, Fabiana Rampazzo, Carlo de Santi, F Medjdoub, Gaudenzio Meneghesso, et al.

► To cite this version:

Zhan Gao, Matteo Meneghini, Kathia Harrouche, Riad Kabouche, Francesca Chiocchetta, et al.. Short term reliability and robustness of ultra-thin barrier, 110 nm-gate AlN/GaN HEMTs. *Microelectronics Reliability*, 2021, 123, pp.114199. 10.1016/j.microrel.2021.114199 . hal-03287632

HAL Id: hal-03287632

<https://hal.science/hal-03287632v1>

Submitted on 15 Jul 2021

HAL is a multi-disciplinary open access archive for the deposit and dissemination of scientific research documents, whether they are published or not. The documents may come from teaching and research institutions in France or abroad, or from public or private research centers.

L'archive ouverte pluridisciplinaire **HAL**, est destinée au dépôt et à la diffusion de documents scientifiques de niveau recherche, publiés ou non, émanant des établissements d'enseignement et de recherche français ou étrangers, des laboratoires publics ou privés.

Short Term Reliability and Robustness of ultra-thin barrier, 110 nm-gate AlN/GaN HEMTs

Zhan. Gao¹, Matteo. Meneghini¹, Kathia Harrouche², Riad Kabouche², Francesca Chiocchetta¹, Etienne Okada², Fabiana. Rampazzo¹, Carlo. De Santi¹, Farid Medjdoub², Gaudenzio. Meneghesso¹, Enrico. Zanoni¹

¹Dipartimento di Ingegneria dell'Informazione, Università di Padova, Via Gradenigo 6/A, 35131 Padova

²CNRS-IEMN, Institut d'Electronique, de Microélectronique et de Nanotechnologie, 59652 Villeneuve-d'Ascq, France

Email :gaozhan.veronica@gmail.com

Abstract—Short-term reliability and robustness of 110 nm AlN/GaN HEMTs has been evaluated by means of off-state, semi-on state and on-state step stress tests on devices having different gate-drain distance, L_{GD} . While breakdown voltages and critical voltages scale almost linearly with L_{GD} , failure mode remains almost unchanged in all tested devices, and consists in an increase of gate leakage, accompanied by a positive shift of threshold voltage. In off-state, electroluminescence images detect the presence of localized leakage paths which may act as preferential paths for electron trapping. Degradation is therefore preliminary attributed to hot-electron trapping, enhanced by electric fields.

Keywords—AlN/GaN HEMTs, reliability, stress, breakdown mechanism, electric field, radio frequency

I. INTRODUCTION

GaN-based High Electron Mobility Transistors (HEMTs) have drawn great attention due to their potential for high temperature, high frequency and high power applications to radar amplifiers or modern telecommunication systems as 5G [1]. In order to achieve power density and power added efficiency at high frequency, up to Q-band, one of the most usual approaches is to scale the gate length of the devices [2], but this would lead to short channel effect. Therefore, it is necessary to optimize the epilayer design and the device layout, and reduce the gate to channel distance [3]. Recently, AlN/GaN heterostructures have been proven to be able to reach a maximum current of 2.3 A/mm and peak transconductance of 480 mS/mm [4], and state-of-the-art PAE over > 65% at 40 GHz [5], by adopting an ultra-thin (3-4 nm) AlN barrier. Good stability and robustness have been achieved by AlN/GaN/AlGaIn HEMTs for Ka band operation during constant voltage stress tests [6]. Reliability of AlN/GaN HEMTs with 4 nm AlN barrier during constant voltage stress has been also studied at room temperature and high temperature [7], [8]. However, available data on the reliability and robustness of AlN/GaN HEMTs are still scarce. Effective on-wafer evaluation methods are needed during device development in order to provide a fast feedback on the different technological options.

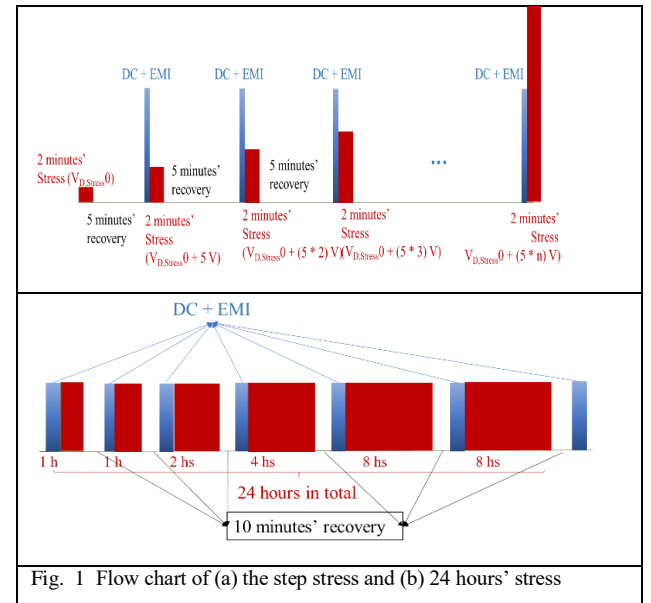
In this work, we focus on the short-term reliability of a new generation ultra-scaled AlN/GaN HEMTs with 3 nm AlN barrier, and with 110 nm-gate length, grown on SiC substrates. Parametric degradation and breakdown effects observed during drain voltage step stress tests were studied at three states: (1) off-state ($V_{GS} = -5$ V), (2) semi-on state ($V_{GS} = -1$ V), and (3) on-state ($V_{GS} = 0$ V), as well as an off-state constant voltage at ($V_{GS} = -5$ V, $V_{DS} = 40$ V) stress test. Degradation and robustness of the HEMTs designed with different gate-drain distance (L_{GD}) were compared. Results proved that the new short channel, ultra-thin barrier devices have an excellent device robustness. Electroluminescence imaging technique was used to have an insight in device

behavior during stress. In Section II, the experimental details and the characterization procedures used on the fabricated devices are described. In Section III, a parametric comparison during stress among devices with different L_{GD} are shown, and the degradation mechanism during stress is discussed, in the end of the section, comments on the device breakdown voltages are described.

II. EXPERIMENTAL DETAILS

Tested structures were fabricated on AlN/GaN heterostructures grown on SiC wafers, with an AlN layer thickness of 3 nm and a GaN channel thickness of 100 nm, grown by MOCVD on top of a carbon doped GaN buffer. In order to reduce surface trapping and better protect the surface, a 10 nm in-situ SiN layer was grown on top. More experimental details can be found in [5].

The devices under test are two-fingers with gate length (L_G) of 0.11 μm , gate width (W_G) of $2 \times 50 \mu\text{m}$; gate-drain distances (L_{GD}) are designed to be 0.5 μm , 1.5 μm and 2.5 μm . The maximum current of the devices is around 1.2 A/mm and the maximum transconductance is up to 400 mS/mm for the fabricated devices. Cut off frequency (f_T) and maximum oscillation frequency (f_{max}) achieved at $V_{DS} = 20$ V are 63 GHz and 300 GHz, respectively. A more thorough DC and RF characterization is discussed in [5].



In this work, drain step stress tests at off state ($V_{GS} = -5$ V), semi-on state ($V_{GS} = -1$ V) and on-state ($V_{GS} = 0$ V) were carried out on devices with different L_{GD} . During stress, drain voltage was increased from 0 V to 200 V or up to catastrophic breakdown in 5 V steps, every two minutes long. During each stress step, drain and gate currents as well

as EL intensity were monitored. After each stress step, the devices were kept unbiased for 5 minutes, and a standard

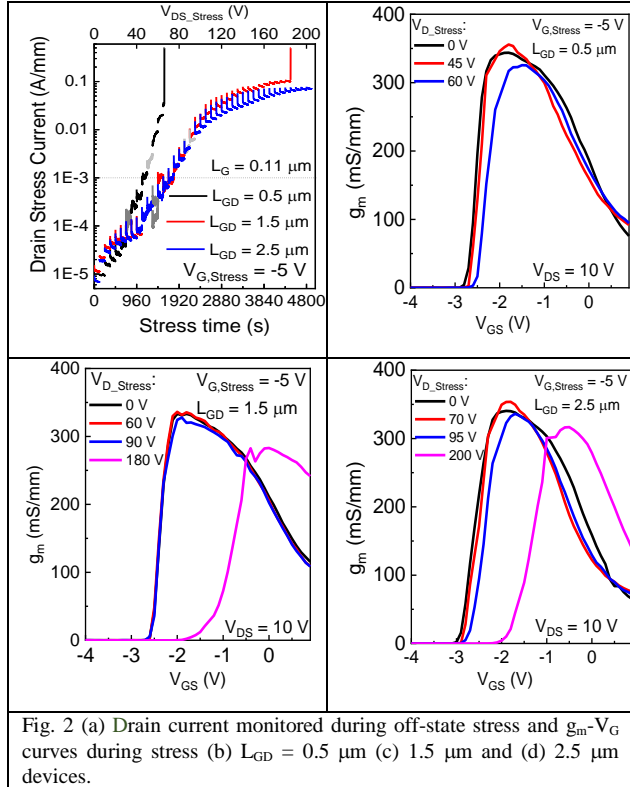


Fig. 2 (a) Drain current monitored during off-state stress and g_m - V_G curves during stress (b) $L_{GD} = 0.5 \mu\text{m}$ (c) $1.5 \mu\text{m}$ and (d) $2.5 \mu\text{m}$ devices. DC characterizations were taken afterwards, as shown in Fig. 1 (a). A second group of devices was submitted to a constant voltage stress test at off-state ($V_{GS} = -5 \text{ V}$, and $V_{DS} = 40 \text{ V}$), in order to evaluate the devices reliability on a short time scale. The flow chart of the 24 hours stress is summarized in Fig. 1(b). DC characteristics degradation after the 24 hours' stress among devices having different L_{GD} was summarized and compared.

III. RESULTS

A. Off-state drain step stress

Device drain current recorded during off-state stress ($V_G = -5 \text{ V}$) is shown in Fig. 2 (a) for the different L_{GD} : $0.5 \mu\text{m}$, $1.5 \mu\text{m}$ and $2.5 \mu\text{m}$. Device with $L_{GD} = 2.5 \mu\text{m}$ did not show catastrophic failure up to 200 V , while $L_{GD} = 0.5 \mu\text{m}$ and $1.5 \mu\text{m}$ devices suffered destructive breakdown at 70 V and 185 V , respectively. If one adopts a failure criteria corresponding to a drain leakage current density of 1 mA/mm , the following failure voltages are obtained, respectively for $L_{GD} = 0.5 \mu\text{m}$, $1.5 \mu\text{m}$ and $2.5 \mu\text{m}$ devices: 45 V , 60 V and 70 V . The increase in leakage current is usually caused by the generation of preferential leakage current conduction paths.

As the step stress proceeds, a positive threshold voltage shift occurs; in the $L_{GD} = 1.5 \mu\text{m}$ device, V_{th} shift reaches approximately 1.5 V , at the same time transconductance g_m shows a decrease of 16% at the 180 V step. It should be noted, however, that V_{TH} shift is negligible and that no degradation of I_{Dsat} or g_m occurs until the stress voltage reaches 50 V , 85 V and 90 V , for $L_{GD} = 0.5 \mu\text{m}$, $1.5 \mu\text{m}$ and $2.5 \mu\text{m}$ devices, respectively.

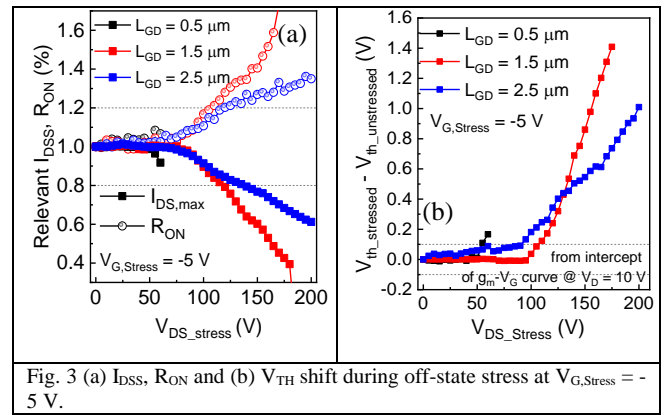


Fig. 3 (a) I_{DSS} , R_{ON} and (b) V_{TH} shift during off-state stress at $V_{G,Stress} = -5 \text{ V}$.

The g_m - V_G curves at $V_D = 10 \text{ V}$ of the devices after the critical stress steps are shown in Fig. 2 (b)-(d). Maximum drain current (I_{DSS}), ON resistance (R_{ON}) and threshold voltage (V_{TH}) evolution during stress are shown in Fig. 3. It is worth noticing that in $L_{GD} = 0.5 \mu\text{m}$ devices there is no significant parametric degradation until sudden breakdown, when the drain stress voltage is over 65 V . I_{DSS} decrease and R_{ON} increase started from 85 V and 90 V , for $L_{GD} = 1.5 \mu\text{m}$ and $2.5 \mu\text{m}$ devices, respectively. The I_{DSS} decrease and V_{TH} shift can be explained by trapping effects under the gate, possibly under the channel or in the buffer.

Electroluminescence images of the device with $L_{GD} = 0.5 \mu\text{m}$, $1.5 \mu\text{m}$ and $2.5 \mu\text{m}$ taken before stress and after stress at ($V_G = -5 \text{ V}$, $V_D = 45 \text{ V}$, 60 V and 70 V) are shown in Fig. 4. Before stress, there is no hot spots along the finger, after 2 minutes' stress at 45 V , 60 V and 70 V , EL image showed leakage points along the gate finger, thus demonstrating the generation of localized leakage paths during stress, possibly in correspondence to defects which may also act as trapping centers.

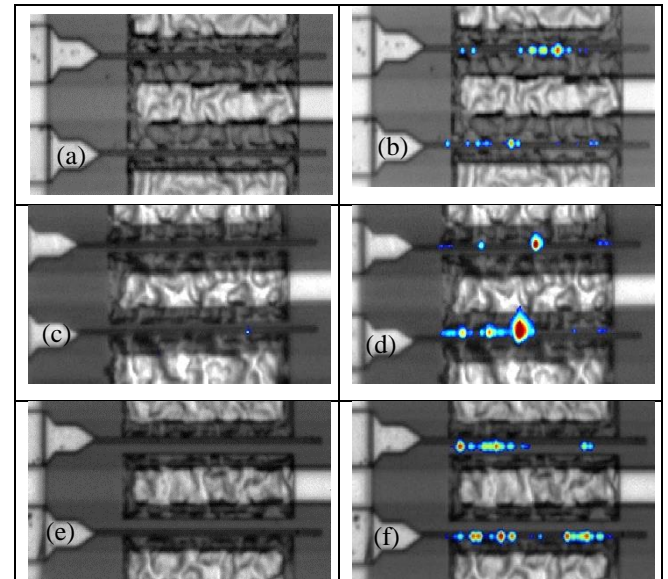
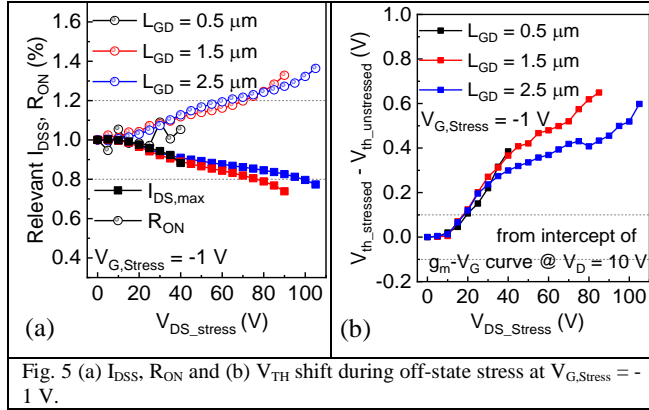


Fig. 4 emission images (15 s emission) of the $L_{GD} = 0.5 \mu\text{m}$ device (a) before stress at ($V_G = -5 \text{ V}$, $V_D = 0 \text{ V}$), and (b) during stress at ($V_G = -5 \text{ V}$, $V_D = 45 \text{ V}$); the $L_{GD} = 1.5 \mu\text{m}$ device (c) before stress at ($V_G = -5 \text{ V}$, $V_D = 0 \text{ V}$), and (d) during stress at ($V_G = -5 \text{ V}$, $V_D = 60 \text{ V}$) and the $L_{GD} = 2.5 \mu\text{m}$ device (e) before stress at ($V_G = -5 \text{ V}$, $V_D = 0 \text{ V}$), and (f) during stress at ($V_G = -5 \text{ V}$, $V_D = 70 \text{ V}$).

B. Semi-on state drain step stress

Drain and gate currents of the devices with different L_{GD} recorded during semi on-state stress ($V_G = -1$ V) are shown in Fig. 7. Devices with $0.5 \mu\text{m}$, $1.5 \mu\text{m}$ and $2.5 \mu\text{m}$ L_{GD} showed catastrophic failure at 50 V, 95 V and 110 V, respectively. Channel current decreases during the step stress tests, possibly due to the combined effect of device self-heating and electron trapping. The gate leakage current reached 1 mA/mm at stress voltages of 35 V, 65 V and 100 V, for $0.5 \mu\text{m}$, $1.5 \mu\text{m}$ and $2.5 \mu\text{m}$ devices, respectively.



The transconductance curves of the devices at $V_D = 10$ V after some stress steps are shown in Fig. 7 (b)-(d). Different from what was observed during off-state stress, I_{DSS} decreased gradually, R_{ON} increased gradually, and V_{TH} showed gradual positive shift with increasing stress voltage in all devices, regardless of L_{GD} , as shown in Fig. 5. The $L_{GD} = 2.5 \mu\text{m}$ device showed the largest maximum transconductance decrease at the step before breakdown,

No leakage current increase was observed until the stress voltage exceeded 25 V, 35 V and 35 V for $0.5 \mu\text{m}$, $1.5 \mu\text{m}$ and $2.5 \mu\text{m}$ devices, respectively, in agreement with the gate leakage current change observed during stress.

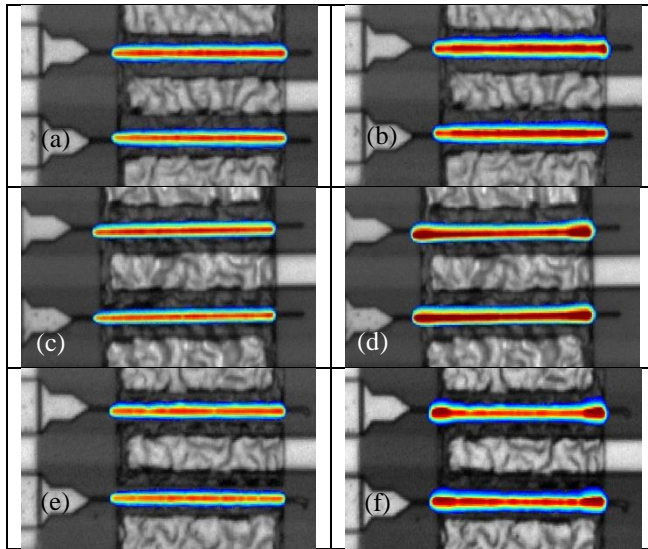


Fig. 6 emission images (15 s emission) of the $L_{GD} = 0.5 \mu\text{m}$ device (a) at ($V_G = -1$ V, $V_D = 20$ V), and (b) during stress at ($V_G = -1$ V, $V_D = 30$ V); the $L_{GD} = 1.5 \mu\text{m}$ device (c) at ($V_G = -1$ V, $V_D = 20$ V), and (d) during stress at ($V_G = -1$ V, $V_D = 40$ V) and the $L_{GD} = 2.5 \mu\text{m}$ device (e) at ($V_G = -1$ V, $V_D = 20$ V), and (f) during stress at ($V_G = -1$ V, $V_D = 40$ V).

The EL images of the devices with $L_{GD} = 0.5 \mu\text{m}$, $1.5 \mu\text{m}$ and $2.5 \mu\text{m}$ taken during stress at stress ($V_D = 20$ V) and after stress at ($V_D = 40$ V) are shown in Fig. 6. Even EL intensity distribution can be observed along gate fingers during tests at $V_D = 20$ V, as shown in Fig. 6(a) (c) (e). At higher drain voltages, emissions are stronger at finger extremes, as carrier transport is worsened by device self-heating in the central part of the device.

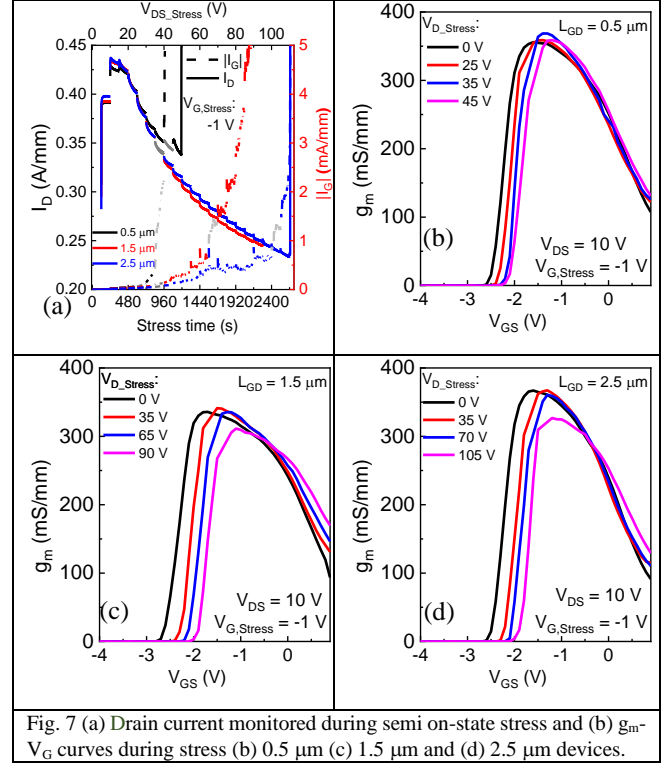
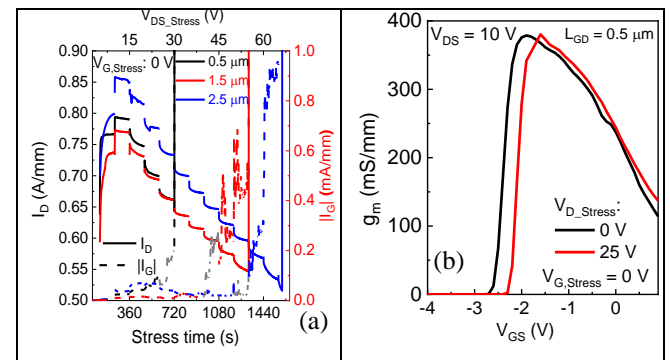


Fig. 7 (a) Drain current monitored during semi on-state stress and (b) $g_m - V_G$ curves during stress (b) $0.5 \mu\text{m}$ (c) $1.5 \mu\text{m}$ and (d) $2.5 \mu\text{m}$ devices.

C. On-state drain step stress

Drain and gate current of the devices recorded during on-state stress are shown in Fig. 8 (a). Despite the very large power density ($15 \text{ W/mm}^2 \approx 30 \text{ W/mm}^2$), devices with $0.5 \mu\text{m}$, $1.5 \mu\text{m}$ and $2.5 \mu\text{m}$ of L_{GD} did not fail up to burnout occurring at 30 V, 55 V and 65 V, respectively. The failure mechanism is most possibly due to thermal effect caused by device self-heating.



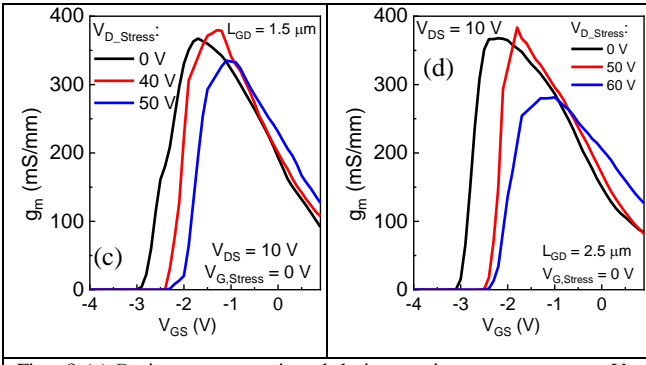


Fig. 8 (a) Drain current monitored during semi on-state stress, g_m - V_G curves during stress (b) $0.5 \mu\text{m}$ (c) $1.5 \mu\text{m}$ and (d) $2.5 \mu\text{m}$ devices.

The g_m - V_G curves of the devices at $V_D = 10 \text{ V}$ after several stress steps are shown in Fig. 8(b)-(d). Similar to the semi-on state stress, $g_{m,max}$ decrease occurred at the last stress step before breakdown, and the devices with stress step before breakdown, and the devices with the $2.5 \mu\text{m}$ L_{GD} have most $g_{m,max}$ degradation.

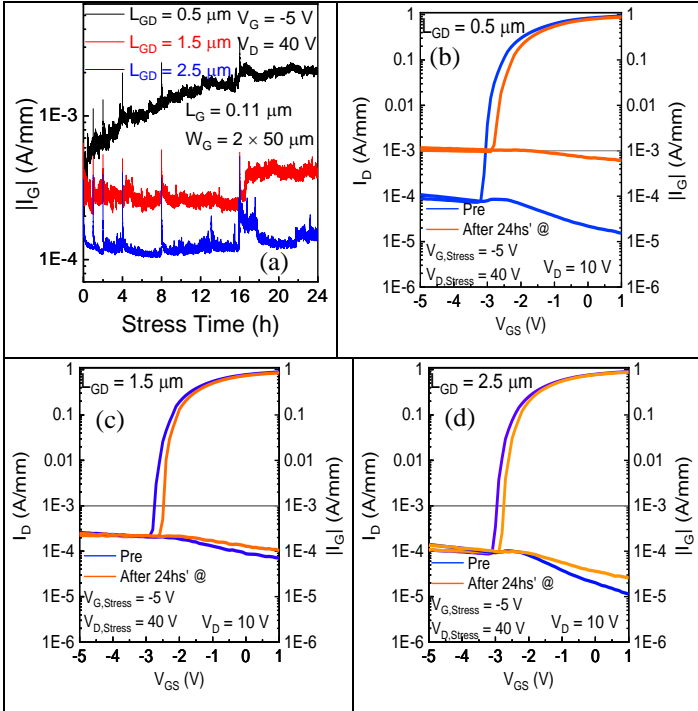


Fig. 11 (a) Drain current monitored during constant voltage stress, I_D - V_G curves during stress (b) $0.5 \mu\text{m}$ (c) $1.5 \mu\text{m}$ and (d) $2.5 \mu\text{m}$ devices.

V_{TH} shifts positively with increasing stress voltage, with comparable shift in devices with different L_{GD} , possibly due to traps under the gate in the buffer or at gate edges, whose occupation and effect does not depend on the gate-drain distance, as shown in Fig. 9.

Leakage current increase can be observed, at 25 V , 40 V and 50 V for $0.5 \mu\text{m}$, $1.5 \mu\text{m}$ and $2.5 \mu\text{m}$ devices, consistent with the gate leakage current increase monitored during stress.

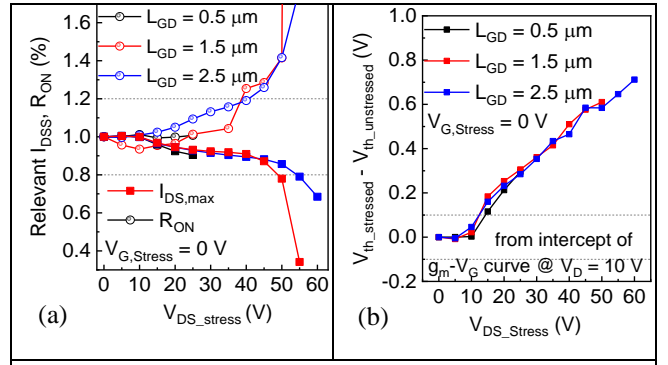


Fig. 9 (a) I_{DSS} , R_{ON} and (b) V_{TH} shift during off-state stress at $V_{G,Stress} = 0 \text{ V}$.

Erreur ! Source du renvoi introuvable. shows breakdown voltages V_{BR} and critical voltage V_{CRI} (The voltage where leakage current exceeds 1 mA/mm) of the AlN/GaN HEMTs with difference L_{GD} . DC short-term safe operating area for the three different gate-drain spacings are also shown. It should be noted that, despite the thin barrier layer (3 nm AlN) and short channel length (110 nm), devices with the shortest L_{GD} reach off-state $V_{BR} = 70 \text{ V}$, $V_{CRI} = 55 \text{ V}$ (50 V and 35 V in semi-on, on state) and can withstand a DC dissipated power as high as $P_D = 15 \text{ W/mm}$ in on-state.

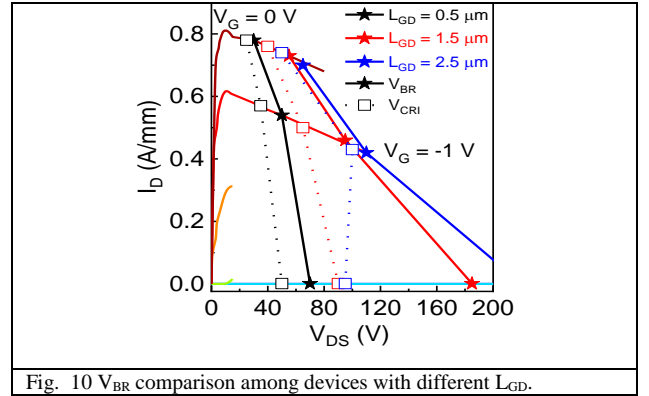


Fig. 10 V_{BR} comparison among devices with different L_{GD} .

D. Constant Voltage stress- off state

In order to evaluate the reliability of the devices under operating conditions, constant voltage stress tests in the off-state condition $V_G = -5 \text{ V}$, $V_D = 40 \text{ V}$ were carried out. DC characteristics were measured at room temperature before, during (at each step) and after the stress.

Drain and gate leakage current during stress are shown in Fig. 11. Leakage current reached 1 mA/mm after four hours' stress for the device with $0.5 \mu\text{m}$ of L_{GD} , possibly due to the leakage path caused by trapping effects assisted by high electric field at the gate edge. The device with $1.5 \mu\text{m}$ and $2.5 \mu\text{m}$ of L_{GD} showed less than one order of magnitude increase in leakage current after 24 hours' stress.

The I_D - V_G curves of the devices at $V_D = 10 \text{ V}$ before and after 24 hours' stress are shown in Fig. 11(b)-(d). The $L_{GD} = 0.5 \mu\text{m}$ devices showed one order of magnitude increase in leakage current, a value in agreement with the leakage current increase observed during stress. The threshold voltage shifted positively by $+0.3 \text{ V}$. The g_m - V_G

curves in Fig. 12(a) showed that there is no $g_{m,max}$ decrease during stress.

For the devices with $L_{GD} = 1.5 \mu\text{m}$, there is almost no leakage current increase, similar to that observed during stress. The transfer characterization $I_D V_G$ in Fig. 11(c) and $g_m V_G$ curves in Fig. 12 (b) showed that the degradation signature of the devices is V_{th} positive shift (+0.2 V). For the devices with $L_{GD} = 2.5 \mu\text{m}$, no leakage current increase or maximum transconductance increase is observed, similar to the device with $L_{GD} = 1.5 \mu\text{m}$, and the V_{TH} shift is close to +0.18 V.

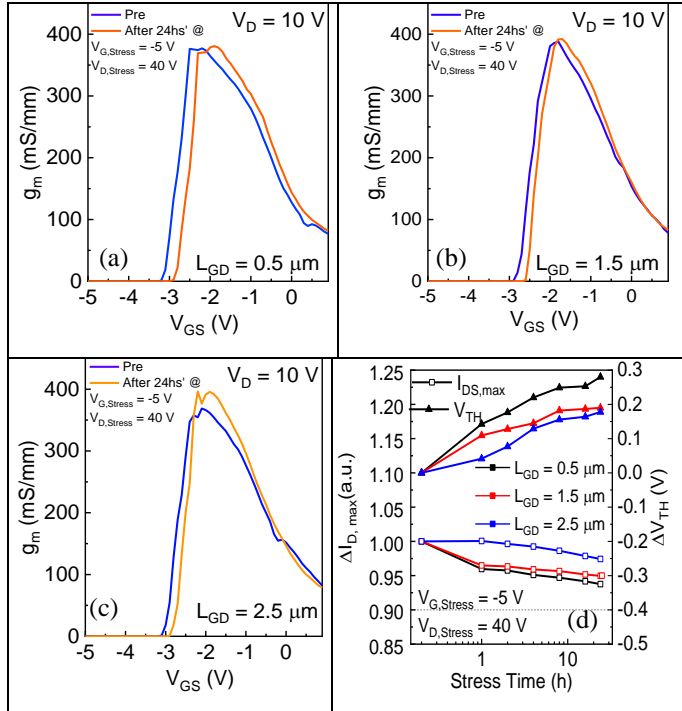


Fig. 12 Transfer $g_m V_G$ curves during stress of (a) $0.5 \mu\text{m}$ (b) $1.5 \mu\text{m}$ and (c) $2.5 \mu\text{m}$ devices and (d) I_{DSS} and V_{TH} shift during constant voltage stress at $V_{G,Stress} = -5 \text{ V}$, $V_{D,Stress} = 40 \text{ V}$.

The I_{DSS} decrease and V_{TH} shift during stress are summarized in Fig. 12 (d). The I_{DSS} decrease is less than 10%, and I_{DSS} degradation percentage and V_{TH} shift showed a dependence on L_{GD} .

Electroluminescence images of the three kinds of devices taken during the first 15 s and after 24 hours stress at ($V_G = -5 \text{ V}$, $V_D = 40 \text{ V}$) are shown in Fig. 13. Five hot spots occurred as soon as stress started for the $0.5 \mu\text{m}$ device, three hot spots can be observed for the $1.5 \mu\text{m}$ device, and one hot spot can be observed for the $2.5 \mu\text{m}$ device. After stress at (-5 V , 40 V) for 24 hours, EL image showed many new leakage points along the gate finger. Therefore, this demonstrates that the generation of localized leakage paths during stress, possibly in correspondence to defects which may also act as trapping centers.

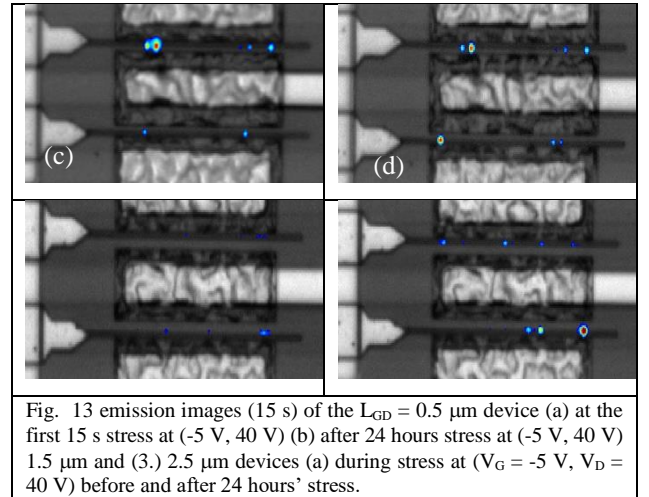
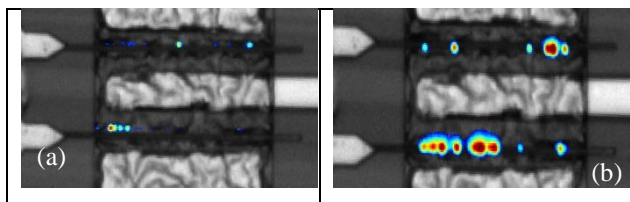


Fig. 13 emission images (15 s) of the $L_{GD} = 0.5 \mu\text{m}$ device (a) at the first 15 s stress at (-5 V , 40 V) (b) after 24 hours stress at (-5 V , 40 V) $1.5 \mu\text{m}$ and (3.) $2.5 \mu\text{m}$ devices (a) during stress at ($V_G = -5 \text{ V}$, $V_D = 40 \text{ V}$) before and after 24 hours' stress.

IV. DISCUSSIONS AND CONCLUSIONS

From the results shown in the previous section, positive threshold voltage shift and leakage current increase has been observed during all the stress processes, regardless of bias voltage (off state, semi-on state and on state). Maximum transconductance decrease was observed at the step before breakdown during semi-on and on state stress, and the degradation percentage depends greatly on L_{GD} .

The V_{TH} shift during the off-state stress could be explained by trapping effects under the gate, traps could be generated in the GaN buffer far below the 2DEG [9], result from vacancy migration under high electric field [10], or can be related to the carbon doping in the GaN buffer [11].

Another explanation could be that during off state stress, electron tunneling occurs at the drain edge of the gate, and electrons are injected into the surface-state layer and captured by the surface deep donors, or charges at the SiN/AlN interface [12], hereby, the 2DEG density is decreased due to these negative surface charges, leading to V_{TH} positive shift [13].

In conclusion, short-term reliability and robustness of 110 nm AlN/GaN HEMTs has been evaluated by means of off-state, semi-on state and on-state step stress tests and a constant voltage stress at off-state on devices having different gate-drain distance, L_{GD} . While breakdown voltages and critical voltages scale almost linearly with L_{GD} , failure mode remains almost unchanged in the nine device groups, and consists in an increase of gate leakage, accompanied by a positive shift of threshold voltage. In off-state, electroluminescence images detect the presence of localized leakage paths which may correspond to dislocations and act as preferential paths for electron trapping. Degradation is therefore preliminary attributed to trapping effects, enhanced by electric field, as shown in [14], [15].

ACKNOWLEDGEMENT

Support by EUGANIC project under the EDA Contract B 1447 IAP1 GP, by the EC Horizon 2020 ECSEL project 5G_GaN_2, by the ESA ESTEC project RELGAN, and by the Italian Ministry of University and Research (MIUR), PRIN project GANAPP is gratefully acknowledged.

REFERENCES

- [1] U. K. Mishra, P. Parikh, W. Yi-Feng, and Y. F. Wu, "AlGaIn/GaN HEMTs—an overview of device operation and applications," *Proc. IEEE*, vol. 90, no. 6, pp. 1022–1031, 2002.
- [2] G. H. Jessen *et al.*, "Short-channel effect limitations on high-frequency operation of AlGaIn/GaN HEMTs for T-gate devices," *IEEE Trans. Electron Devices*, vol. 54, no. 10, pp. 2589–2597, 2007.
- [3] D. Marti, S. Tirelli, A. R. Alt, J. Roberts, and C. R. Bolognesi, "150-GHz cutoff frequencies and 2-W/mm output power at 40 GHz in a millimeter-wave AlGaIn/GaN HEMT technology on silicon," *IEEE Electron Device Lett.*, vol. 33, no. 10, pp. 1372–1374, 2012.
- [4] T. Zimmermann *et al.*, "AlN/GaN Insulated-Gate HEMTs With 2.3 A/mm Output Current and 480 mS/mm Transconductance," *Electron Device Lett. IEEE*, vol. 29, no. 7, pp. 661–664, 2008.
- [5] K. Harrouche, R. Kabouche, E. Okada, and F. Medjdoub, "High Performance and Highly Robust AlN/GaN HEMTs for Millimeter-Wave Operation," *IEEE J. Electron Devices Soc.*, vol. 7, no. 1, pp. 1145–1150, 2019.
- [6] G. Meneghesso *et al.*, "First Reliability Demonstration of Sub-200-nm AlN/GaN-on-Silicon Double-Heterostructure HEMTs for Ka-Band Applications," *IEEE Trans. Device Mater. Reliab.*, vol. 13, no. 4, pp. 480–488, Dec. 2013.
- [7] T. Kemmer *et al.*, "Voltage- and Temperature-Dependent Degradation of AlN/GaN High Electron Mobility Transistors," in *2018 International Integrated Reliability Workshop (IIRW)*, 2018, vol. 2018-October, pp. 1–6.
- [8] M. Rzin *et al.*, "Linearity and robustness evaluation of 150-nm AlN/GaN HEMTs," *Microelectron. Reliab.*, vol. 100–101, no. June, p. 113388, Sep. 2019.
- [9] Z. Zhang *et al.*, "Correlation of proton irradiation induced threshold voltage shifts to deep level traps in AlGaIn/GaN heterostructures," *J. Appl. Phys.*, vol. 119, no. 16, pp. 2–8, Apr. 2016.
- [10] K. H. Warnick, Y. Puzyrev, T. Roy, D. M. Fleetwood, R. D. Schrimpf, and S. T. Pantelides, "Room-temperature diffusive phenomena in semiconductors: The case of AlGaIn," *Phys. Rev. B*, vol. 84, no. 21, p. 214109, Dec. 2011.
- [11] A. Chini *et al.*, "Experimental and Numerical Analysis of Hole Emission Process from Carbon-Related Traps in GaN Buffer Layers," *IEEE Trans. Electron Devices*, vol. 63, no. 9, pp. 3473–3478, 2016.
- [12] M. Meneghini *et al.*, "Negative Bias-Induced Threshold Voltage Instability in GaN-on-Si Power HEMTs," *IEEE Electron Device Lett.*, vol. 37, no. 4, pp. 474–477, Apr. 2016.
- [13] M. Faqir, G. Verzellesi, G. Meneghesso, E. Zanoni, and F. Fantini, "Investigation of high-electric-field degradation effects in AlGaIn/GaN HEMTs," *IEEE Trans. Electron Devices*, vol. 55, no. 7, pp. 1592–1602, 2008.
- [14] R. Jiang *et al.*, "Multiple Defects Cause Degradation After High Field Stress in AlGaIn/GaN HEMTs," *IEEE Trans. Device Mater. Reliab.*, vol. 18, no. 3, pp. 364–376, Sep. 2018.
- [15] J. Bergsten *et al.*, "Electron Trapping in Extended Defects in Microwave AlGaIn/GaN HEMTs with Carbon-Doped Buffers," *IEEE Trans. Electron Devices*, vol. 65, no. 6, pp. 2446–2453, 2018.